DLITE: Dynamic Local Intercellular Tension Estimation

R. Vasan[1], M.M. Maleckar[2], C.D. Williams [*2] and P. Rangamani[†1]

[1]Department of Mechanical and Aerospace Engineering, University of California San Diego, San Diego, CA, 92122

[2]Allen Institute for Cell Science, Seattle, WA, 98109

February 5, 2019

Abstract

The shape of cell-cell interfaces and the forces resulting from actomyosin interactions, membrane tension, or cell-cell adhesion are closely coupled. For example, the tight junction protein, ZO-1, forms a link between the force-bearing actin cortex and the rest of the tight junction protein (TJP) complex, regulating epithelial cell differentiation and the flux of solutes across epithelia. Here we introduce a method for Dynamic Local Intercellular Tension Estimation (DLITE) to computationally infer the evolution of cell-cell forces from a mechanical model of collective cell behaviour. This builds upon prior work in the field (CellFIT, Brodland et al., PloS one 9.6 (2014): e99116). We validate our estimated forces against those predicted by Surface Evolver simulations. Inferred tensions of a cell colony rearranging over time correlate better with the ground truth for our method (DLITE) than for prior methods intended for single time-points. DLITE is robust to both skeletonization errors and topological changes. Finally, we used DLITE in WTC-11 human induced pluripotent stem (hIPS) cells endogenously expressing ZO-1 GFP to find that major topological changes in cell connectivity, e.g. mitosis, can result in an increase in tension. This suggests a correlation between the dynamics of cell-cell forces and colony rearrangement.

Keywords Optimization, Force, Tension, ZO-1, Colony, Cells

[*]cdavew@alleninstitute.org

[†]prangamani@ucsd.edu

Introduction

Morphological processes during tissue remodeling events such as wound healing [1], development [2], expansion [3], migration [4, 5] and cancer invasion [6] involve mechanical cell-cell rearrangements driven by physical forces. Cells transmit these forces through intercellular cell-cell junctions via adhesion complexes such as adherens junctions [7] and tight junctions [8]. These multimolecular complexes, found in the apical cell cortex [9], depend on the activity of the actomyosin cytoskeleton [10, 11]. The mechanotransduction of cell-cell forces can further alter and regulate signalling pathways [12, 13].

The dynamics of tissue reshaping is crucial to collective cell behaviour, commonly evidenced by the intercalation and extrusion of cells during development or apoptosis in cell cultures [14, 15]. This dynamic remodeling of cell-cell contacts has previously been suggested to be functionally mechanical, driven by actomyosin cortical line tension in the junctions [16, 17]. While it is clear that membrane-actomyosin interactions are necessary for dynamic morphogenetic behaviour, the nature of these forces and membrane tension remains poorly understood.

To elucidate the role of tension in tissue remodeling, one can utilize force measurement techniques such as atomic force microscopy (AFM), traction force microscopy (TFM), micro-pipette aspiration etc [18]. However, these techniques are disruptive [19] and not always amenable towards measurements at apical junctional complexes. Förster Resonance Energy Transfer (FRET) tension probes appear to be an alternative [20–22], but are limited to smaller force ranges and rely on the assumption of a constant force-stretch calibration curve [21].

Alternatively, force can be non-disruptively inferred across colonies by mechanically balancing a given colony shape using computational methods [23–25]. For such a computational method to result in accurate estimates of force – *first*, the method must be able to take into account the irregular, curved shapes of cell-cell junctions (Fig. 1A) and *second*, the method must be able to predict the dynamic evolution of the forces during colony rearrangement. The irregularity in the shape of cell-cell junctions requires the use of curvilinear methods of edge handling (Fig. 1B). CellFIT is the current state of the art force-inference technique for applications across cell colonies [23]. However, CellFIT does not predict the dynamic evolution of cell-cell force, which is critical since edge and vertex locations in colonies constantly change. Here we develop a method that implements a local minima time series extension of CellFIT. We named this method Dynamic Local Intercellular Tension Estimation, or DLITE. In

what follows, we describe the model underlying DLITE and applications to cell colony dynamics. We show DLITE, in addition to enabling predictions of colony tension over time, increases robustness of force estimation during digitization errors. We end the study with application of DLITE to time series of human induced pluripotent stem (hIPS) cell lines with the endogenously GFP-labeled tight junction protein ZO-1 and discuss how inference tools can complement experimental measurements in cell biology.

Methods

Assumptions

We employed a curvilinear description of a tissue by defining a colony as a directed planar graph comprising cells (c), edges (e) and nodes (n) (Fig. 1B, for more details see SOM and [23, 26]). Forces exerted by the actomyosin cortex result in tangential stresses in the form of tension (t) along an edge. Cells resist deformation by means of a normal stress exerted as pressure (p) inside every cell. Along each edge, we assumed that the interfacial tensions are constant and that the intracellular pressures are uniform within a cell. At the length scale of the whole cell, we ignored membrane bending and assumed that edge tensions and cell pressures exclusively govern cell shape. We treated viscous forces as negligible and therefore assumed that the colony shape is quasi-static.

Governing equations and system specification

A general force balance at every node in a colony can be written as (Fig. 1B)

$$n_{\text{residual}} = \underbrace{\left| \sum_{i=1}^{e_n} t_i v_i \right|}_{\text{(Tension balance per node)}} , \tag{1}$$

where n is a node, t, and v represent the tension/tangential stress and local tangent unit vector of an edge connected to node n respectively, e_n is the number of edges connected to node n and n_{residual} is the magnitude of the resultant tension vector coming into a node (ideally 0). This equation is complete when employing a curvilinear description of tissue and applies to a node that is *(i.)* connected to at least three edges and *(ii.)* in mechanical equilibrium [23]. The pressure difference between adjacent cells can be estimated using Laplace's law as

$$e_{\text{residual}} = \underbrace{p_i - p_j - \frac{t}{r}}_{\text{(Pressure balance per edge)}} \quad , \tag{2}$$

where e is an edge, p_i and p_j are the pressure of adjacent cells i and j respectively and e_{residual} is the residual error from the pressure balance. Here, t and r represent the tension and radius of the interfacial edge e. The system of equations for tension and pressure are generally overdetermined; there is no unique solution to this system [23]. Therefore, we can only predict the relative distribution of tensions.

To compute the dynamics of cell-cell forces, we reformulated the tension balance (Eq. 1) as a local optimization problem defined as

$$\underset{t}{\text{minimize}} \quad f(t) = \sum_{j=1}^{N} \left(n_{\text{j,residual}} + \underbrace{\frac{n_{\text{j,residual}}}{\sum_{i=1}^{e_{n_j}} \mid t_i v_i \mid}}_{\text{Regularizer}} \right), \tag{3}$$

where n_j and e_{n_j} represent the jth node and the number of edges connected to node n_j, and N is the total number of nodes in the colony. Here, $n_{j,\text{residual}}$ is the tension residual at a given node (Eq. 1) and the regularizer is the magnitude of the tension residual divided by the sum of the magnitude of the tension vectors coming into that node. Since tension cannot be negative, we set a lower tension bound of zero. In Eq. 3, the regularized term ensures that the system of equations does not converge to a globally trivial solution (tension = 0 along all edges) [27]. Pressure in each cell was computed using

$$\underset{p}{\text{minimize}} \quad g(p) = \sum_{j=1}^{E} e_{j,\text{residual}}^2, \tag{4}$$

where E is the total number of edges in the colony and e$_j$ is the residual error from the pressure balance at the jth edge. Tension and pressure solutions were normalized to an average of 1 and 0 respectively, similar to prior work [23–25]. In contrast to previous methods, DLITE uses the values of tension at each edge and pressure in each cell from the previous time point as an initial guess for the current timepoint. This mode of time stepping in the optimization procedure enables us to use information from previous time points to predict the values of tension and pressure at the current time point and forms the basis of DLITE.

Tracking nodes and edges

A notable component of DLITE is the ability to provide an initial guess for every edge tension and every cell pressure independently, allowing us to incorporate a time history of cell-cell forces. However, this requires node, edge, and cell tracking over time. We implemented this tracking by randomly assigning labels to nodes, edges, and cells at the initial time point. Then, nodes were tracked by assigning the same label to the closest node at the next time point. Edges were tracked by comparing edge angles connected to nodes with the same label and cells were tracked by matching cell centroid locations across time. Our model optimization pipeline was implemented using Scipy's unconstrained optimization algorithm 'Limited-memory Broyden–Fletcher–Goldfarb–Shanno (L-BFGS)' [28]. The global optimization technique 'Basinhopping' was used to seek a global minimum solution at the first time point [29].

Results

DLITE allows us to use the tension at a specific cell-cell junction at a given time point as an initial guess to calculate tensions at the next time point. This logical progression then allows us to infer forces over time that demonstrate a strong correlation to ground truth values for model geometries. We demonstrate robustness and sensitivity of DLITE by validating it against ground-truth tensions for multiple synthetic geometries, multiple tension perturbations within a colony, skeletonization errors at single or multiple time points, and topological changes like the shrinkage of cell-cell contacts. At each point, we compare predictions to those produced by the state of the art CellFIT technique. We then apply DLITE to movies of skeletonizations of endogeneously tagged tight junction ZO-1 (*zonulae occludentes* - 1) in an hIPS cell line and predict dynamic cell-cell forces during colony dynamics.

Validation of DLITE as a dynamic tension-inference tool

We validated DLITE in three steps. First, we compared edge tension and cell pressure solutions obtained using our implementation of the CellFIT algorithm and DLITE to ground truth values in synthetic geometries made available via the current version of CellFIT called ZAZU (Fig. S1). We reimplemented the CellFIT algorithm in Python because the source code of ZAZU is not publicly available. Both our reimplementation of CellFIT (Fig. S1B) and DLITE (Fig. S1C) perform identically

with respect to the ground truth for single frames (Fig. S1A), with an average error of ~ 0.02 (Fig. S1D).

Second, to generate time-series synthetic data, we needed to simulate colonies that deformed smoothly across time. We used Surface Evolver to do this [30]. Surface Evolver relaxes an initial geometry into its minimum energy configuration through gradient descent. This energy (W) was defined as

$$W = \underbrace{\sum_{j=1}^{E} t_j L_j}_{\text{Tension energy}} + \underbrace{\sum_{k=1}^{C} p_k A_k}_{\text{Pressure energy}} , \tag{5}$$

where t_j, L_j are the tension and length of the jth edge and p_k, A_k are the pressure and area of the kth cell respectively. E and C are the total number of edges and cells in the colony (see SOM for details). Here, the tension energy represents a net energy contribution due to adhesion forces that stabilize a cell-cell interface and actomyosin cortical tensions that shorten cell-cell contacts. Pressure was enforced as a Lagrange multiplier. Initial geometries were first created from random Voronoi tessellations followed by Lloyd relaxation [31]. In order to generate a time-series, we performed multiple Evolver simulations where the tension of a few randomly selected edges were either increased or decreased between time points (Fig. 2A). Edge tensions at each time point were static and the average tension was normalized to 1. We then stripped all tension and pressure information from the resulting shapes and used these shapes as input to our method. Using DLITE and CellFIT separately, we inferred colony forces and compared the two approaches (Fig. 2B, D). Initially, both methods performed identically, but showed divergence after 3 frames. Importantly, we observed that the values of tension predicted using our method stick closer together over time and are better correlated (r = 0.94 (DLITE) vs r = 0.75 (CellFIT)) to the ground truth (Fig. 2 B, D). Further, we observed that the stochasticity in tension or change in edge tension over time (Δtension) using DLITE also correlates better to the ground truth change in edge tension (Fig. 2C).

Third, to ensure robustness, we tested multiple tension perturbations in the same geometry (Fig. S2) and perturbations in other randomly generated geometries (Fig. S3). In all cases, we observed equivalent or better correlation of both the tension and change in edge tension with the ground truth using DLITE when compared to CellFIT.

DLITE is robust to skeletonization errors

The input to a force-inference model is a map of colony shape as a series of curved edges and the nodes where edges join. Segmentation transforms image data into information about the isolated geometric structures. Subsequently, skeletonization methods extract lines that characterize the topology and connectivity of the tension bearing network in the colony. Errors in this mapping present challenges to force inference techniques that rely on accurate colony connectivity and edge tracing [23–25]. New methods have improved the quality of predicted network topology and connectivity; both deep learning models and traditional computer vision techniques have made significant advances in 2D/ 3D biological segmentations [32–35]. Despite these advances, current skeletonization methods continue to require semi-manual post-processing because of ambiguities present in the structures during imaging and added by the image apturing modalities employed. This semi-manual cleanup is increasingly impractical for larger colonies and time series. As a result, we require force-inference techniques that are robust to such mapping errors. As we demonstrate below, our inference method has increased robustness to such edge/ node mapping errors, decreasing the number of manual corrections required, and making the inference of forces in time series tractable. Here we evaluate the effects of edge/ node mapping errors on force-inference in *(i.)* a single image and *(ii.)* a time-series.

We first analyzed, at a single time point, the effect of a commonly occurring connectivity error, where the intersection between two edges is missing. We generated a synthetic colony image to initialize the system with known edge tensions. Fig. 3A shows a random Voronoi tessellation generated using Surface Evolver where 50 edges (out of 330 total) have larger values of tension than others. The ground truth tensions were the inputs given to Surface Evolver (Fig. 3A). A single edge was deliberately traced incorrectly to introduce a skeletonization error. This error resulted in the loss of a triple junction and breaking the integrity of a cell. Since the node of interest is now connected to two edges instead of three, we can no longer conduct a tension balance at that location. This results in a badly conditioned tension matrix and CellFIT can no longer infer a correct distribution of tensions along the remaining two edges (Fig. 3A&B). However, because the DLITE approach balances edge tension on a node-by-node basis, it reduces the effect of local tension errors on the global data set. As a result, we find that at a given time point, DLITE is able to provide a good estimate of the tension of the neighboring edges (Fig. 3C, see also Fig. S4).

Another commonly occurring skeletonization error results from poor estimation of edge curvature

due to incorrect values of between-edge angles at a particular node. This is especially problematic for stray edges along the boundary of the colony as the tension residual per node is inversely correlated to the number of connected edges (Fig. S5A). To simulate this, we decreased the tension of a few edges along the boundary of a colony (Fig. S5B). Decreasing the tension leads to an increased edge curvature consistent with Eq. 5. These modified edges become non-circular at very low tensions. As a result, they are no longer compatible with circular arc fitting to determine the edge intersection angles. A consequence of this incompatibility is that the tension residuals are large and the tension distributions obtained using CellFIT are incorrect (Fig. S5C). However, DLITE is able to predict the correct distribution of tensions in this case when compared with the ground truth (Fig. S5D). The reasons for this are two-fold: first, DLITE infers small tension residuals at all non-boundary edges and second, it is not poorly scaled by errors in local tension.

Finally, we considered a class of mapping challenges that are present only in time-series data – identification of edges from one frame to the next. Misidentification of edges frequently occurs when an edge is lost for a single frame, severing the edge's connection to its prior label. Fig. 3D shows a time-series with a missing edge (edge label 33) and two missing cells at time point 8. The missing edge leads to the loss of a triple junction, and consequently, CellFIT predicts incorrect tensions (Fig. 3E, CellFIT). For tracking purposes, missing an edge also means that the edge that was being tracked up to that point no longer exists, and therefore a new edge label is assigned. Since edges with new labels do not have an initial tension guess from an identical label at prior time points, these edges are given an initial guess for the value of tension equal to the average initial guess of all edges connected to that edge. By using such a scheme, DLITE can predict tension and Δtension that correlates well with the ground truth (Fig. 3E, F). Thus, in both images and movies of colonies, we find that use of information from the surrounding region allows DLITE to better handle skeletonization errors and predict the distribution of cell-cell forces. The time-series in Fig. 3D also has two topological changes at time points 6 and 8 (edge labels 8 and 25 respectively) that result in differences between CellFIT and DLITE (Fig. 3E, F), with DLITE showing better correlation to the ground truth. This is analyzed in more detail in the next section.

DLITE is robust to topological changes

Network topology or the structure of edges and vertices often display changes in time-series data. Handling of a time-ordered network requires the tracking of nodes, edges, and cells over time. This can be done in 2 ways – if, for example, a single edge ceases to exist at a certain time point, we can choose to *(i.)* keep that edge label and assume that it has temporarily left the field of view or *(ii.)* assign new edge labels ensuring that the lost edge label ceases to exist [36]. Here, we choose the second option in order to condition the network based only on the immediately prior time point. Thus, an edge label that could not be tracked after a time point no longer exists and is assigned a new label. These rules were applied to nodes and cells as well.

If the observed topologies of a cellular network are constantly changing, how then does it affect inferred cell-cell forces? To study the effect of topological changes, we take advantage of the fact that decreasing the tension of two edges in a triple junction results in a decrease of the length of the third connected edge in Surface Evolver. Fig. 4A shows an example time series where edge label 15 disappears at time point 18. This single topological change leads to a badly conditioned tension matrix and poor tension inference when CellFIT is used (Fig. 4B, C). However, DLITE retains the correct distribution of tensions at time point 18 (see also Fig. 3E, edge label 25 at time point 8 and Fig. S6A). While this specific network structure led to poorly scaled tensions using CellFIT after a single edge loss, this is not always the case. If, for example, the network connectivity were to result in a well conditioned tension matrix after the topological change (Fig. 3E, edge label 8 at time point 6 and Fig. S6B), then CellFIT is still able to predict the correct distribution of tensions. However, Δtension is less smooth, and both the tension and Δtension still correlate better to the ground truth while using DLITE (Fig. 3E,F and Fig. S6B). Thus, force inference in dynamic network topologies benefits from incorporating a temporal history of cell-cell forces.

Application to ZO-1 tight junctions

The actomyosin cytoskeleton in cell colonies is connected to 2 major junctional complexes – adherens junctions and tight junctions. Tight junctions (or *zonulae occludentes*), in particular, regulate paracellular diffusion through the spaces between cells by forming a selective barrier. Injury of tight junctions can impair barrier function, leading to complications in lungs [37, 38], kidneys [39], eyes [40] or the small intestine [41]. The actin cytoskeleton plays an important role in the regulation of this

barrier function [42], and is connected to the rest of the tight junction complex through ZO-1 (*zonula occludentes*-1) proteins [43, 44]. Recent studies suggest that actin polymerization and transient Rho activation ('Rho flares') act to quickly restore barrier function upon localized ZO-1 loss at cell-cell contacts [45]. Mechanical cues from the polymerization and branching of the actin network can lead to reshaping of tight junctions, resulting in varying barrier phenotypes.

Here, to investigate the role of tension in tight junction morphogenesis, ZO-1 in hIPS cells was tagged at its endogenous locus with mEGFP and visualized using a spinning confocal disk microscope (see SOM for more details). Using a semi-manual skeletonization of the raw images (Fig. 5B), we predicted the evolution of intercellular forces using DLITE (Fig. 5A, C). While there is no ground truth here, we note that the relative distribution of tensions range from 0 to 3, such that the average tension is normalized to 1. The time interval between adjacent time points was 3 minutes. Interestingly, we observed an increase in tension adjacent to a dividing cell immediately after a mitotic event (Fig. 5A, red box) at time point 15. This increase in tension post-mitosis was observed using both methods (Fig. 5C, edge labels 3, 10 and 11), but only after the removal of bad edges during the semi-manual skeletonization process. This step was important to ensure non-poorly scaled CellFIT solutions, such as the ones at time point 2 and 13. Importantly, the stochasticity in tension (Δtension) was reduced when using DLITE (Fig. 5C, D), indicating a smoothness across time. This reduction in Δtension was determined to be sensitive to the time interval. The standard deviation of Δtension across time was significantly reduced at a time lag of 1 frame (3 minutes), but showed no difference between methods for a time lag of 5 frames (15 minutes). A similar behaviour was confirmed in an additional three scenes of the ZO-1 tight junction (Fig. S7).

Discussion

In this study, we have presented a new method, DLITE, that is based on a local optimization of tension residuals to compute dynamic cell-cell forces. We validated the predictive power of DLITE using synthetic geometries generated from Surface Evolver [30] and showed that DLITE performs better than the prior state-of-the-art method CellFIT [23] when used for time-series data. Importantly, this incorporates a framework to track nodes, edges, and cells across time. Additionally, we demonstrated that DLITE is robust to two forms of network connectivity changes common in time series data – *(i.)* skeletonization errors such as missing node connections, poor edge angle estimates, and stray edges,

and *(ii.)* topological changes that occur as cells move and encounter different neighbors. Finally, we applied DLITE to estimate edge tensions in a time-series of ZO-1 tight junctions and found an increase in tension post mitosis. We showed that DLITE displays a reduced Δtension compared to CellFIT, indicating a smoothness across time. We observed this reduction in three other scenes of the ZO-1 tight junction.

The need for dynamic force-inference tools to understand cell shape and colony rearrangement is paramount as morphological processes from wound healing to germ-band extension rely on transient mechanical forces that are difficult to detect experimentally. Traditional force-measurement tools are *(i.)* limited in number, *(ii.)* deformation based and *(iii.)* require *in-vitro* cell-culture preparation on a synthetic substrate. In contrast, gene expression tools that evaluate expression of specific proteins and label cell boundaries are widely available [18]. Establishing a computational framework to compute the dynamics of cell-cell forces allows us to fill some of these gaps and enable data-driven estimation of intercellular forces.

The use of techniques to estimate forces from cell shape is crucial for understanding cellular processes where shape and function are closely related [46–49]. Studies using single cells on patterned substrates have shown cell shape affects the organization of stress fibers and cytoskeletal forces [50–52]. These shape-force interactions occur at different length scales within a single cell and across cells. For example, at the sub-cellular level, membrane tension governs endocytic bud morphology during intracellular membrane trafficking, while at the multi-cellular level it sorts cells in multicellular aggregates [53–55]. Multiple local deformations along a cell-cell interface can result in changing curvature of that junction, translating mechanics and biochemical signals across length scales [56–58]. Membrane tension plays an important role in all these processes [59].

We acknowledge that our current effort is not without its limitations. It is important to note that the tensions calculated using DLITE depend on fitting circular arcs to every edge; albeit also the case with CellFIT . Since cell-cell junctions can sometimes be distinctly non-circular, the inferred tensions will not approach the ground truth in these cases. Additionally, the current implementation of DLITE is not optimized for computation speed in large colonies. Because we implement a local optimization of tension residuals and perform node, edge and cell tracking over time, the speed of implementation is reduced in very large colonies compared to the constrained least square matrix system solved in CellFIT but remains tractable (1 second vs 5 seconds to process a frame from the time series in Fig. 5 on a contemporary laptop). This can be sped up by improving data structures (e.g. using

a doubly connected edge list data structure to classify edges) and tuning sorting and optimization algorithms. However, there is also a significant amount of time spent in manually pruning edges during the semi-manual skeletonization process in order for CellFIT to infer meaningful solutions. Since DLITE can infer meaningful solutions despite bad edges, the time saving that DLITE offers the user in reduced digitization-correction surpasses the increased computational time by more than an order of magnitude.

While our current focus has been on validating DLITE as a proof of concept, future efforts will focus on the use of DLITE to look at dynamic changes in cell-cell forces in larger data sets of ZO-1 tight junctions. Application of this technique will allow the visualization of cell-cell forces during large scale colony reorganization. This will be aided by continued development in automated and crowd-sourced skeletonization techniques, many of which are readily available today.

Competing Interests

The authors declare that they have no competing financial interests.

Acknowledgments

We thank the entire Allen Institute for Cell Science team, who generated and characterized the gene-edited hiPS cell lines and developed image-based assays used in this work. We especially thank the Allen Institute for Cell Science Assay Development team, particularly Irina Mueller for collecting the ZO-1 time series used here and Susanne Rafelski for invaluable discussions and advise. We would like to thank the Allen Institute for Cell Science Animated Cell team and Daniel Toloudis specifically for providing the 3D rendering of ZO-1 cells used in Figure 1. We thank Paul G. Allen, founder of the Allen Institute for Cell Science, for his vision, encouragement and support. We would also like to thank members of the Rangamani lab and Matthew Akamatsu for comments and feedback. This work was partially supported by ARO W911NF1610411 to P.R.

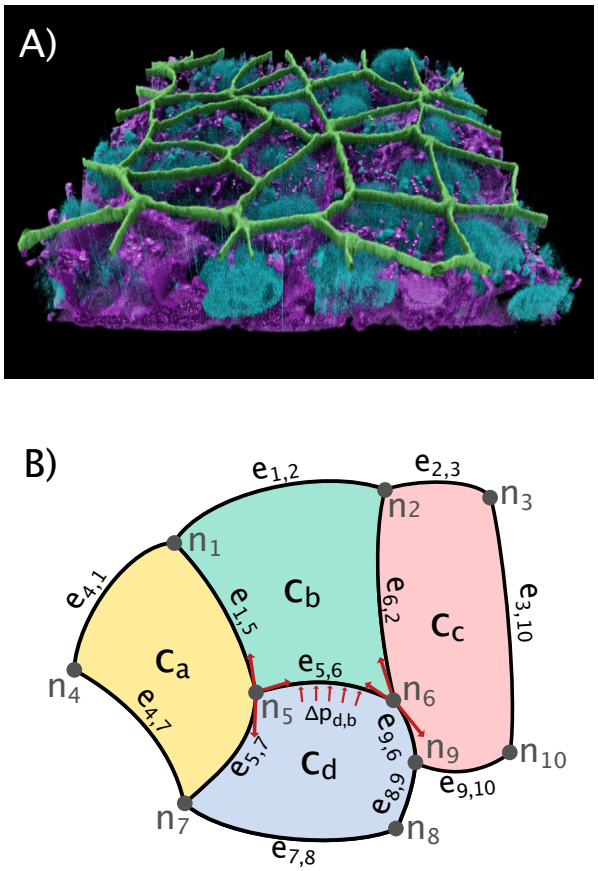

Figure 1: 3D cell view and schematic of tight junction location and force inference technique respectively. (A) 3D view of tight junctions in human induced pluripotent stem (hIPS) cells from the Allen Cell Explorer (Green - Tight junctions, Purple - Membrane, Blue - Nucleus). We predict edge tensions from tight junctions as they localize to the tension bearing apical surface of epithelial-like tissues. (B) Schematic of cell-interface representation used in DLITE and CellFIT force-inference techniques [23]. A colony is represented as a set of nodes (n), edges (e) and cells (c). Edges are directional. Tension balance occurs at each node (red arrows at n_5 and n_6). Pressure difference ($\Delta p_{d,b}$) across a junction is estimated using Laplace's law (red arrows at $e_{5,6}$).

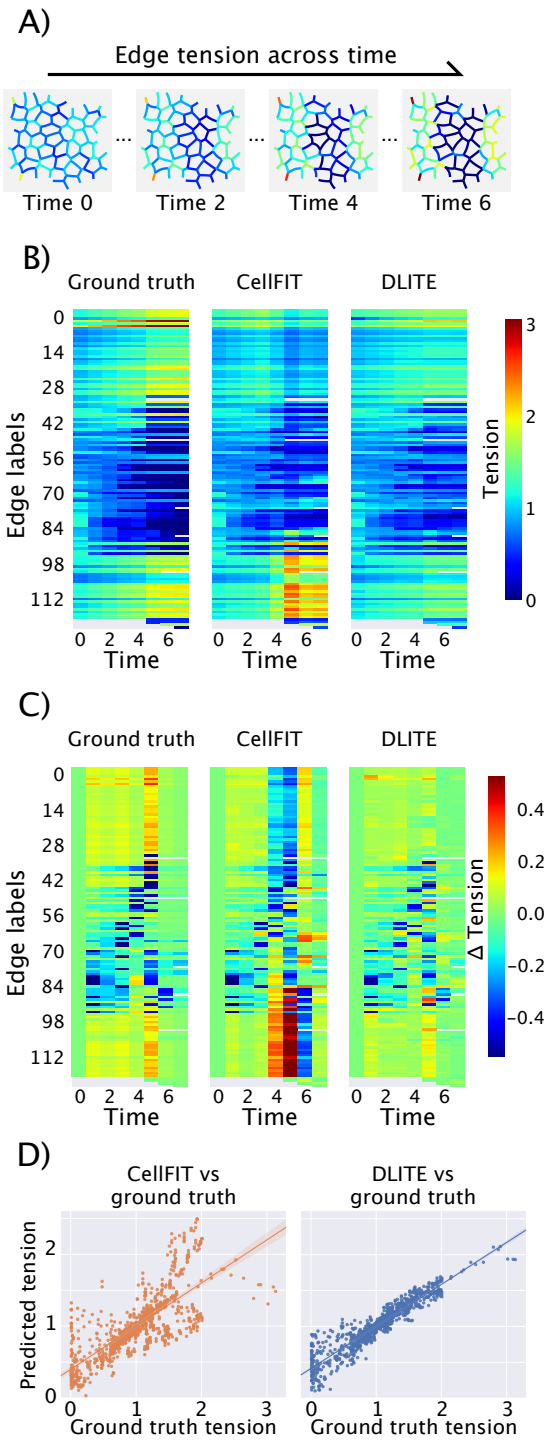

Figure 2: Comparison of DLITE and CellFIT force-inference techniques for ideally digitized time series. Synthetic colonies were generated from random Voronoi tessellations and morphed to minimum energy configurations (Eq. 5) using Surface Evolver [30]. A random set of edges within the colony were perturbed by decreasing or increasing their tensions, resulting in a new colony structure. Repeating this process produced a time-series of colony rearrangement. (A) Time-series of a synthetic colony showing the decrease in tension of 70 edges in the middle of the colony and the increase in tension of 40 edges along the boundary. (B) Heatmap of dynamic edge tensions for ground truth, CellFIT, and DLITE. (C) Heatmap of dynamic change (derivative of tension) in edge tensions for ground truth, CellFIT, and DLITE. (D) Inferred vs ground truth tensions for CellFIT (r = 0.75) and DLITE (r = 0.94). Here, r is the Pearson's correlation coefficient.

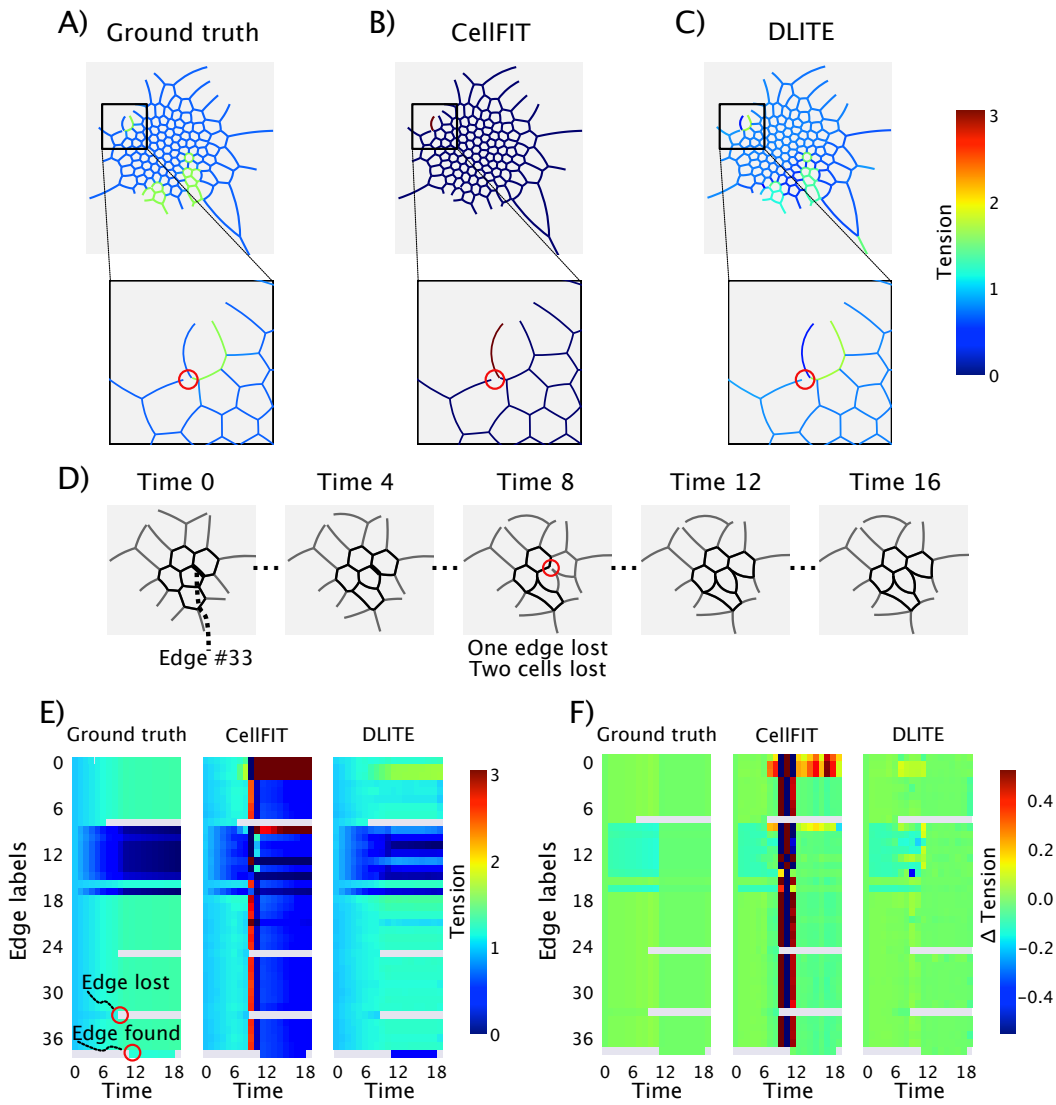

Figure 3: DLITE shows reduced sensitivity to skeletonization errors. (A) Ground truth tensions for a synthetic geometry containing 330 edges generated used Surface Evolver with a single edge connectivity error (circled in red). (B) Tensions computed using CellFIT for the geometry in (A). (C) Tensions computed using DLITE for the geometry in (A). (D) Time-series of a synthetic geometry containing 37 edges generated using Surface Evolver with a single edge connectivity error at time 8 (circled in red). This edge is found again in time step 10 (representing a transient encoding error) but treated as a new edge. (E) Heatmap of dynamic edge tensions for ground truth, CellFIT (r = 0.14) and DLITE (r = 0.87) for the time-series in (D). (F) Heatmap of dynamic change in edge tensions for ground truth, CellFIT, and DLITE for the time-series in (D).

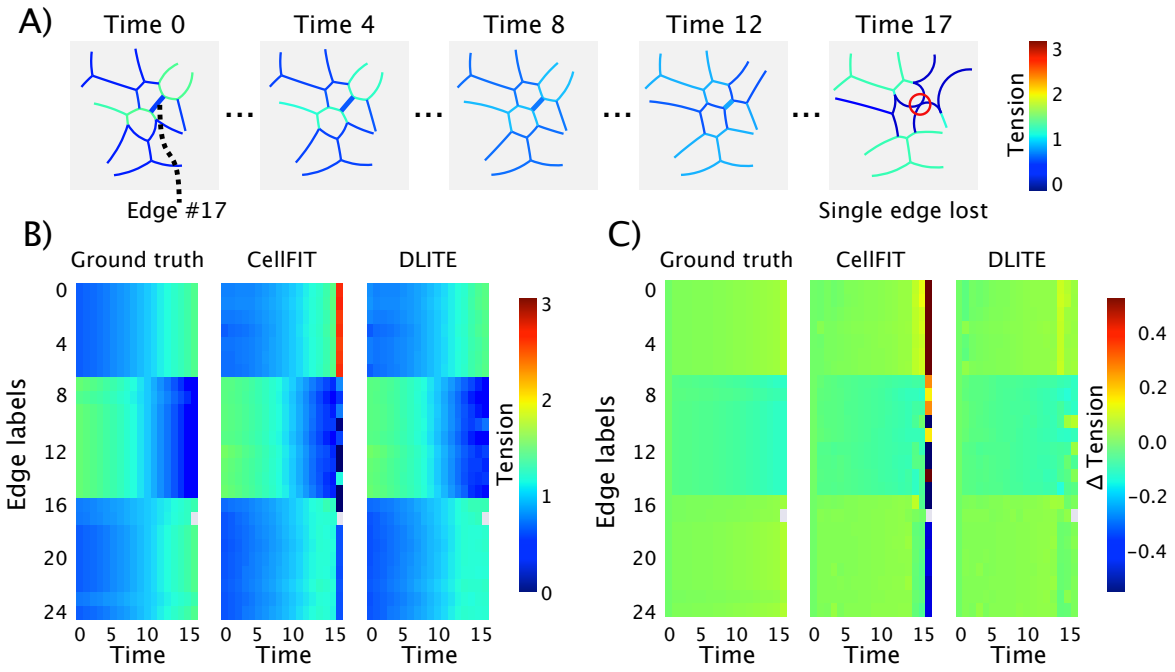

Figure 4: DLITE shows reduced sensitivity to topological changes. (A) Time-series of a synthetic geometry containing 24 edges generated using Surface Evolver where edge label 17 disappears at time 17 (circled in red). (B) Heatmap of dynamic edge tensions for ground truth, CellFIT (r = 0.75), and DLITE (r = 0.98). DLITE shows less disruption to tension prediction on topological change and more closely matches the ground truth tension. (C) Heatmap of dynamic change in edge tensions for ground truth, CellFIT and DLITE.

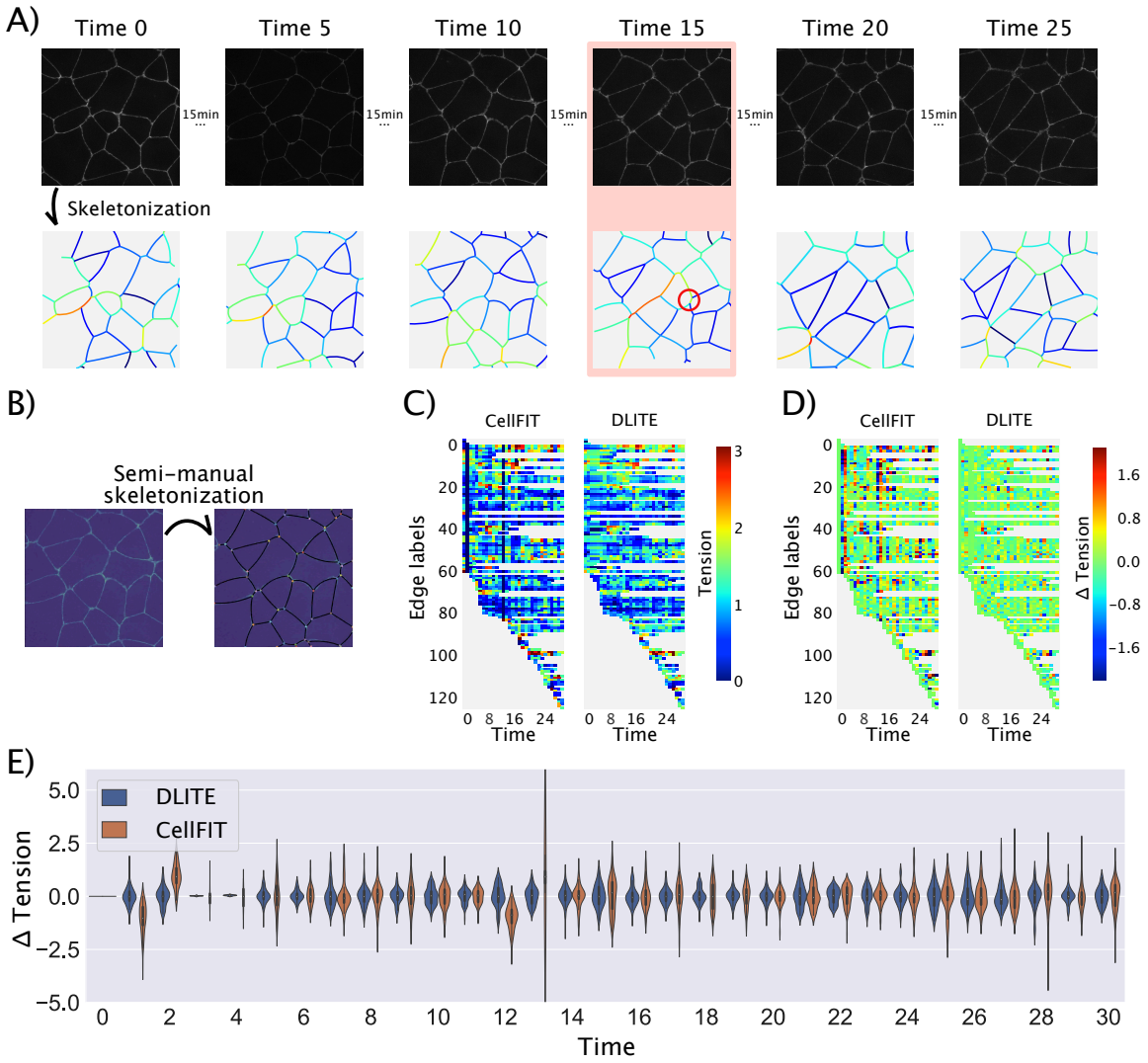

Figure 5: Dynamic cell-cell forces from a time-series of ZO-1 tight junction locations in hIPS cells. DLITE shows reduced fluctuation in tension change, showing more temporally correlated tension predictions. (A) Time-series of ZO-1 GFP images (upper) and dynamics of colony edge tension predicted by DLITE (lower). The following time points are shown: 0, 5, 10, 15, 20 and 25. Time 15 shows an increase in tension along a ridge in the middle of the colony following a mitotic event and the forming of a new edge (circled in red). The time interval between adjacent time points was 3 minutes. (B) Example of a skeletonization of a single raw image of ZO-1 GFP. (C) Heatmap of dynamic edge tensions predicted by CellFIT and DLITE. (D) Heatmap of dynamic change in edge tension predicted by CellFIT and DLITE. (E) Distribution of Δtension at every time point for CellFIT and DLITE.

Supplementary Online Material

Data structures

We implemented our code using the standard scientific Python stack. An object/class groups similar constructs together. Here, we defined 4 main objects - nodes, edges, cells and colonies. Nodes are objects with a unique location (x, y) and node label. Edges are objects that are connected to two unique nodes with a defined edge curvature, direction and edge label. Cells are objects with a unique cell label that contain a particular list of nodes and edges, where a combination of the contained edges forms a cycle. Colonies are objects comprising a list of cells and stray edges (edges that are not part of any cell). Each class has several other defined properties that were useful for time-series tracking and cell-cell force inference.

Curve-fitting

We fit a circular arc to a given list of (x, y) edge co-ordinates using a least squares fitting routine from the Python module Scipy [28].

Cell finding algorithm

Given a list of nodes and edges, we looped through every edge to find the two (or fewer) cells of which each edge might be a part. We started from an initial/current edge and found the next edge that forms the smallest (or largest) angle with the current edge. We repeated this process, setting the new edge as current edge, until the second node of the current edge is the same as the first node of the initial/first edge (indicating a complete cycle). We validated this algorithm in planar graphs generated using the NetworkX module in Python [60]. In pseudocode, this can be formulated as shown in Algorithm 1.

Surface Evolver simulations

Synthetic geometries were generated using the Surface Evolver [30]. In the past, Finite element (FE) models were used to make model geometries, but they do not provide the precision that is possible with Surface Evolver, which is designed to model soap film physics. An initial surface was first defined

Algorithm 1 Cell finding algorithm

```
procedure
    for edge in edges do
        Conn edges ← Network connectivity of edge
        next edge ← max, min angle of Conn edges
        if cellfound then return False
        while cell not found do
            Current edge ← Next edge
            Conn edges ← Network connectivity of Current edge
            next edge ← max, min angle of Conn edges
            if cellfound then return Cell
```

in a datafile comprising a list of vertices, edges, facets and bodies, along with any volume or area constraints for the bodies or facets. Since we defined a 2D string model with a space dimension of 2, we enforced area constraints on the facets instead of volume constraints on the bodies. To generate the datafile, we made random Voronoi tessellations. This was followed by Lloyd relaxation, which results in a more uniform tessellation (as opposed to, for example, a Voronoi tessellation with a single cell significantly bigger than all the other cells). Edges were then assigned random tensions. All cells were assigned the same fixed area in a single simulation (typically 5000). Evolver then uses gradient descent to morph the surface to a minimum energy configuration. This energy (W) was defined as Eq. 5 with the pressure energy enforced as an area constraint. Multiple mesh refinement steps (adjustments of every vertex in the system) were used to ensure a minimum of 10 mesh points along every edge (for better curve-fitting). The evolved geometries were screened for edges that form cell-cell interfaces (as opposed to edges along the boundary that do not form an interface). These edges, along with their corresponding nodes and cells, were stored using our data structures.

In order to generate a time-series, we took a given geometry and perturbed the tension of certain edges. Surface Evolver was used to solve for the minima. This was the next frame t + 1. We repeating this tension perturbation procedure uniformly, such that the geometry is smoothly increasing/ decreasing its curvature at every edge. This correlates to increasing/decreasing tension of every edge (Eq. 5). By stitching together multiple Evolver geometries that progressively showed increasing or decreasing curvature/tension of certain edges, we were able to generate movies of colony rearrangement that was

smooth across time, for whom the ground truth tensions were the input to Surface Evolver.

CellFIT solution

CellFIT [23] evaluates the tension balance as a matrix system defined as

$$G_\gamma \gamma = 0, \tag{6}$$

where γ is a list of surface tension magnitudes and G_γ is a matrix of edge tension coefficients ($\sin$'s and $\cos$'s). Since the system of equations is over-determined, this is formulated as a constrained least squares (Karush Kuhn Tucker or KKT) matrix, which can be written as

$$\begin{bmatrix} G_\gamma^T G_\gamma & C_1^T \\ C_1 & 0 \end{bmatrix} \begin{bmatrix} \gamma_1 \\ \vdots \\ \gamma_N \\ \lambda_1 \end{bmatrix} = \begin{bmatrix} 0 \\ \vdots \\ 0 \\ N \end{bmatrix}, \tag{7}$$

where C_1 = [1, ..., 1], λ_1 is a Lagrange multiplier, and N is the number of edge tensions. This normalizes the average edge tension to 1. Similarly, the pressure balance is evaluated as a matrix system

$$G_p p = q, \tag{8}$$

where p is a matrix of cell pressures and q is a matrix of edge tensions divided by edge curvatures (t/r), as per Laplace's law. This is also formulated as a constrained least squares matrix as

$$\begin{bmatrix} G_p^T G_p & C_2^T \\ C_2 & 0 \end{bmatrix} \begin{bmatrix} p_1 \\ \vdots \\ p_M \\ \lambda_2 \end{bmatrix} = \begin{bmatrix} q_1 \\ \vdots \\ q_M \\ 0 \end{bmatrix}, \tag{9}$$

where C_2 = [1, ..., 1], λ_2 is a Lagrange multiplier and M is the number of cell pressures. This normalizes the average edge pressure to 0.

Force-inference algorithm

In pseudocode, the force-inference algorithm can be formulated as shown in Algorithm 2.

Algorithm 2 Dynamic cell-cell force inference algorithm

```
procedure
    for frame in movie do
        edges, nodes ← trace of image
        cells ← edges, nodes
        colony ← cells
        if labels is empty then return new labels ← nodes, edges, cells
        else tracked labels ← nodes, edges, cells
        if Run computation then
            Add tension residuals or pressure residuals to objective function,
            Update initial guess through labels,
            if first image then return Basinhopping solution
            else L-BFGSB optimization solution
        for node in nodes do
            if conn edges < 3 then return False
            else goto Run computation
        for edge in edges do
            if conn cells < 2 then return False
            else goto Run computation
```

Cell plating for imaging

Human induced pluripotent stem cells (hiPSCs) were plated on glass-bottom multiwell plates (1.5H glass; Cellvis) coated with phenol red–free GFR Matrigel (Corning) diluted 1:30 in phenol red–free DMEM/F12 (Life Technologies). Cells were seeded at a density of 2.5×10^3 in 96-well plates and (12.5–18) imaged 3–4 days later. A detailed protocol can be found at the Allen Cell Explorer (Allen Institute for Cell Science, 2017).

Live-cell imaging

Cells were imaged on a Zeiss spinning-disk microscope with a Zeiss 100×/1.25 W C-Apochromat Korr UV Vis IR objective, a CSU-X1 Yokogawa spinning-disk head, and Hamamatsu Orca Flash 4.0 camera. Microscopes were outfitted with a humidified environmental chamber to maintain cells at 37°C with 5 % CO_2 during imaging. Time-lapse movies were acquired every 3 minutes for 1.5 hours.

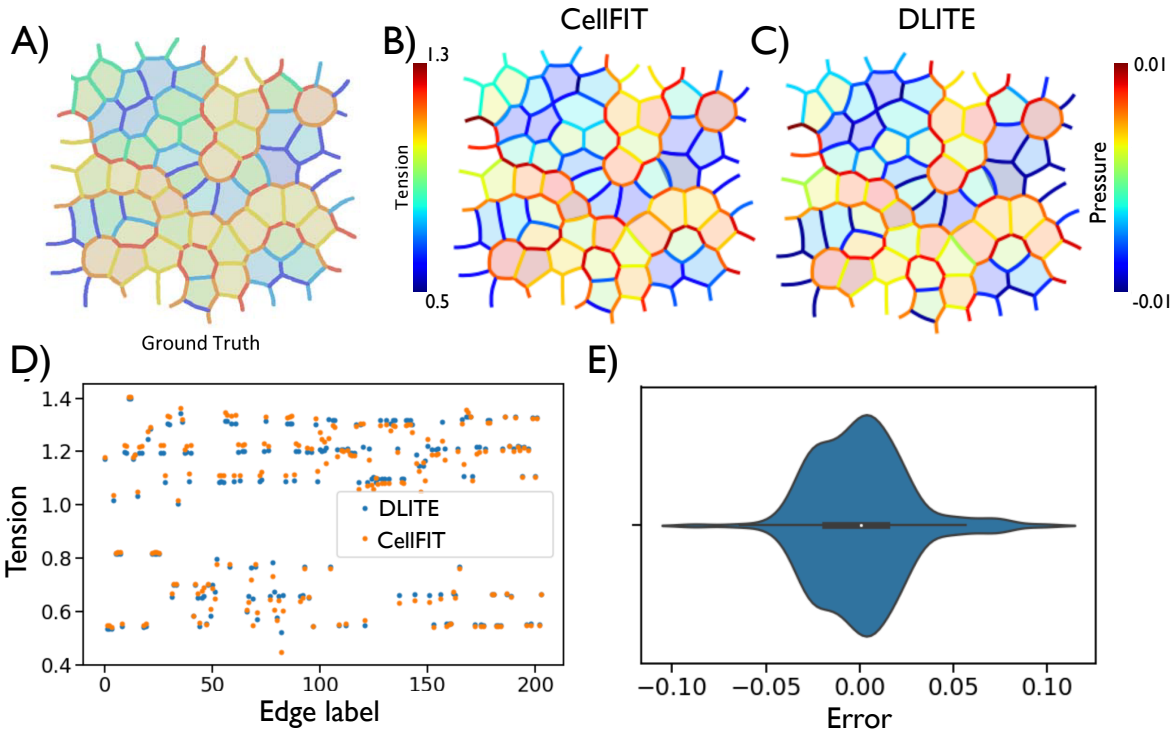

Figure S1: Validation of rewritten CellFIT code. (A) Ground truth geometry used in [23]. (B) Tensions and pressures predicted using CellFIT. (C) Tensions and pressures predicted using DLITE. (D) Tension vs Edge label for CellFIT and DLITE. (E) Error between DLITE tension and CellFIT tension.

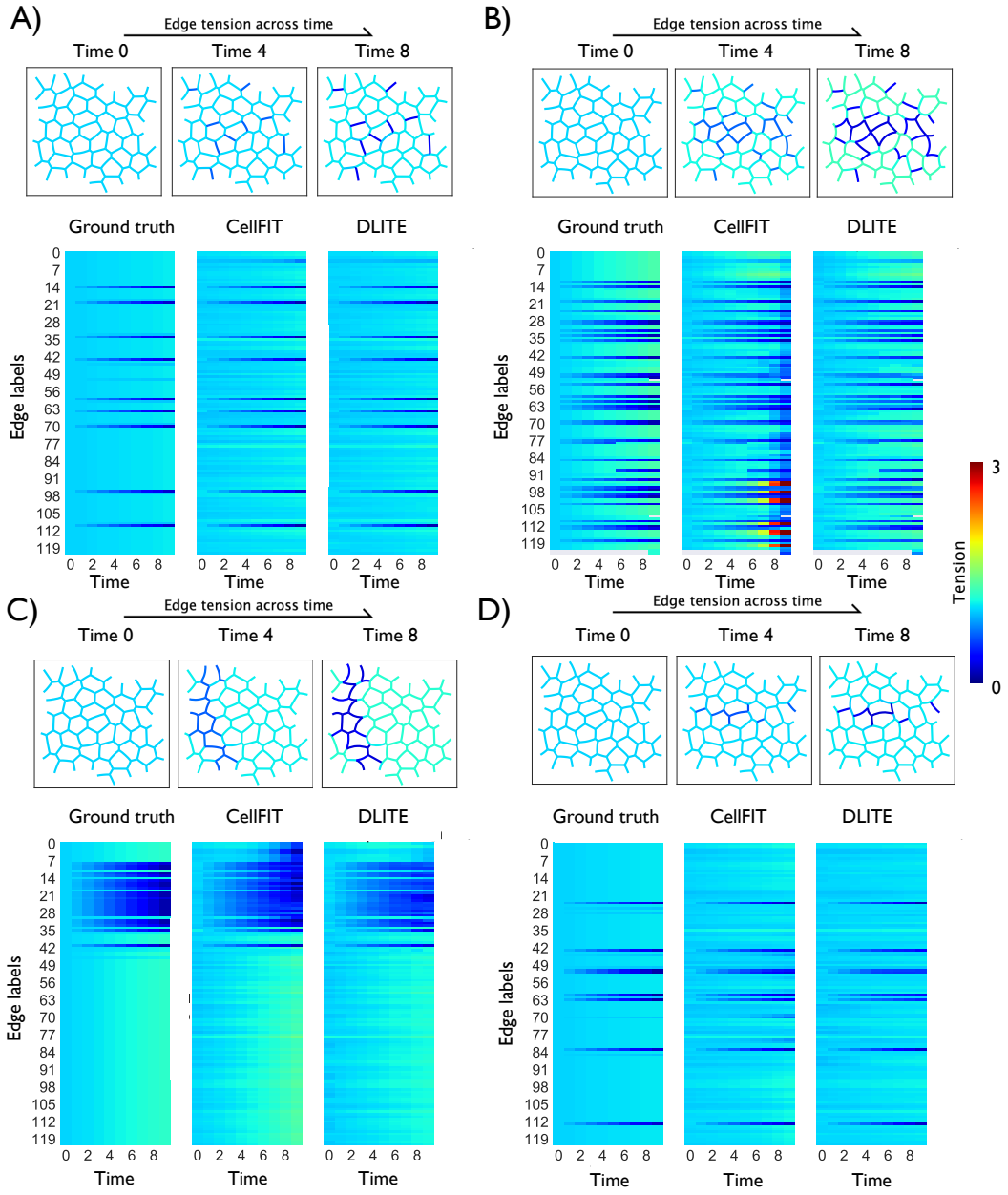

Figure S2: Four example time-series (A-D) of colony rearrangement simulated using four different combinations of decreasing the tension of a few edges and increasing tension of all other edges in the same colony geometry as that in Fig. 2. Average edge tension is normalized to 1 at every time point. Shown - 3 example time points (Time 0, 4 and 8) and heatmaps of dynamic edge tensions for ground truth, CellFIT and DLITE. (A) DLITE - r = 0.97, CellFIT - r = 0.96, (B) DLITE - r = 0.93, CellFIT - r = 0.54, (C) DLITE - r = 0.96, CellFIT - r = 0.86, (D) DLITE - r = 0.94, CellFIT - r = 0.93

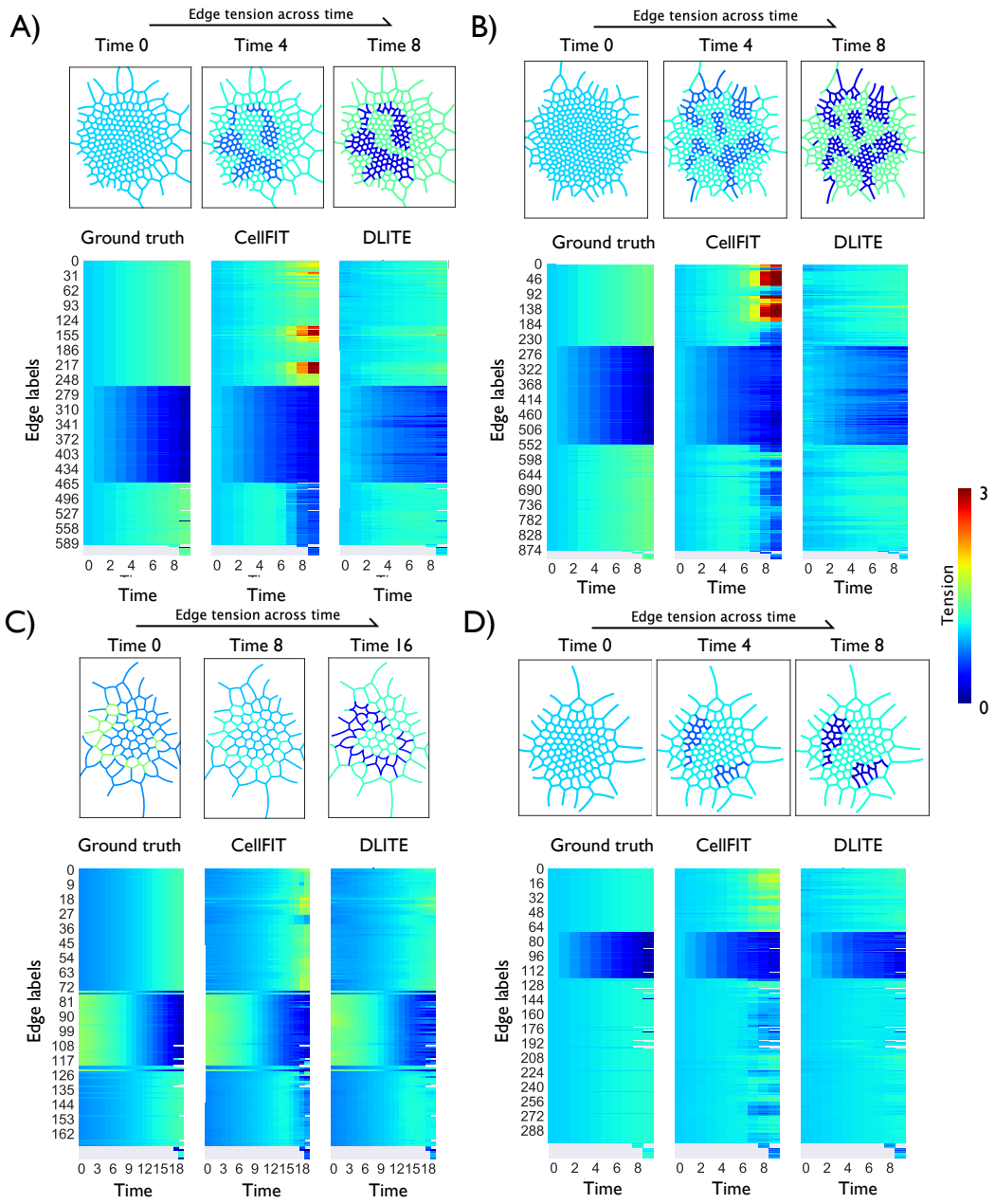

Figure S3: Four example time-series (A-D) of colony rearrangement simulated by decreasing the tension of a few edges and increasing tension of all other edges in four randomly generated colony geometries of different sizes. Average edge tension is normalized to 1 at every time point. Shown - 3 example time points (Time 0, 4 and 8 or Time 0,8 and 16) and heatmaps of dynamic edge tensions for ground truth, CellFIT and DLITE. (A) DLITE - r = 0.94, CellFIT - r = 0.76, (B) DLITE - r = 0.92, CellFIT - r = 0.6, (C) DLITE - r = 0.95, CellFIT - r = 0.9, (D) DLITE - r = 0.96, CellFIT - r = 0.84.

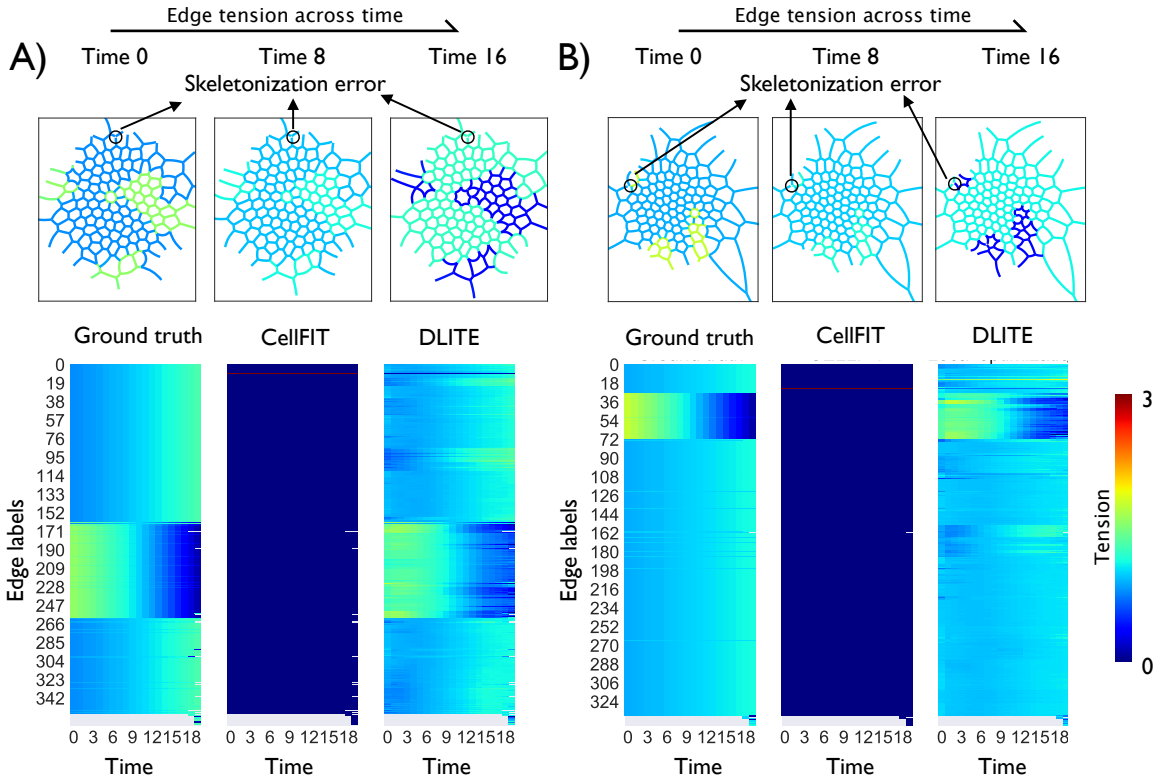

Figure S4: Two example time-series (A, B) of colony rearrangements with single skeletonization errors at a node. Average edge tension is normalized to 1 at every time point. Shown - 3 example time points (Time 0, 8 and 16) and heatmaps of dynamic edge tensions for ground truth, CellFIT and DLITE. (A) DLITE - r = 0.88, CellFIT - r = 0.22, (B) DLITE - r = 0.83, CellFIT - r = 0.25.

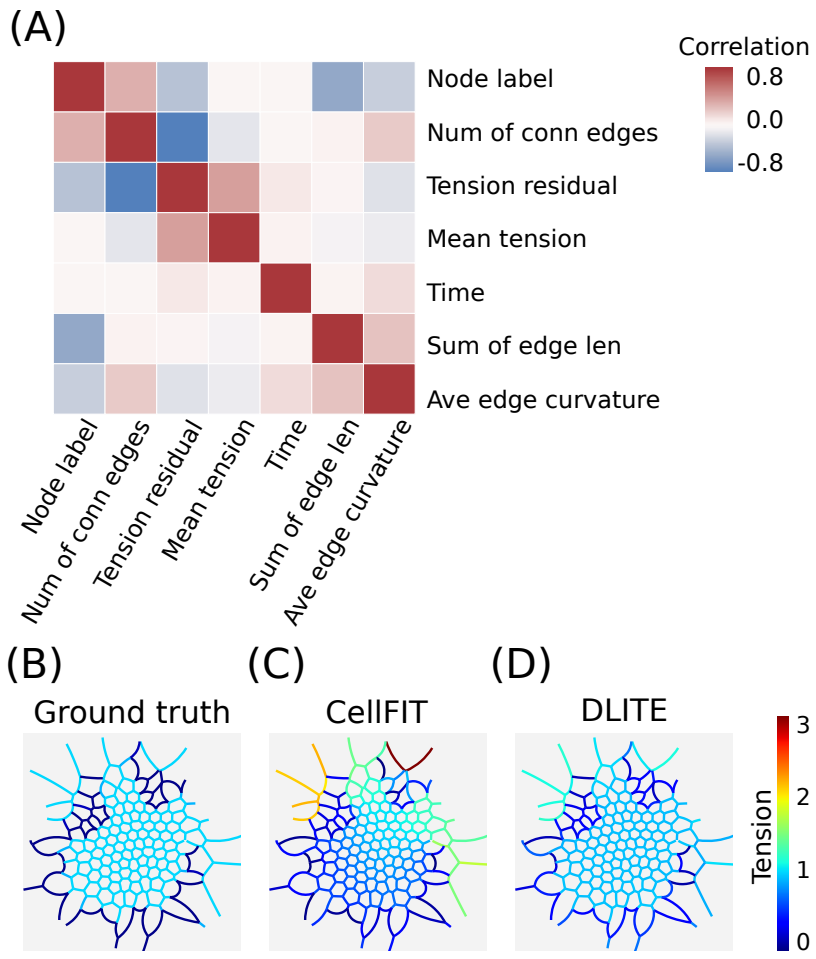

Figure S5: DLITE shows reduced sensitivity to poor tension residual residuals at nodes with fewer number of connected edges. (A) Clustermap depicting negative correlation between the net tension residual and the number of connected edges at any given node. (B) Example synthetic geometry with reduced ground truth tensions along a large number of stray edges. (C) CellFIT tensions (r = 0.34) for geometry in (B). (D) DLITE tensions (r = 0.9) for geometry in (C).

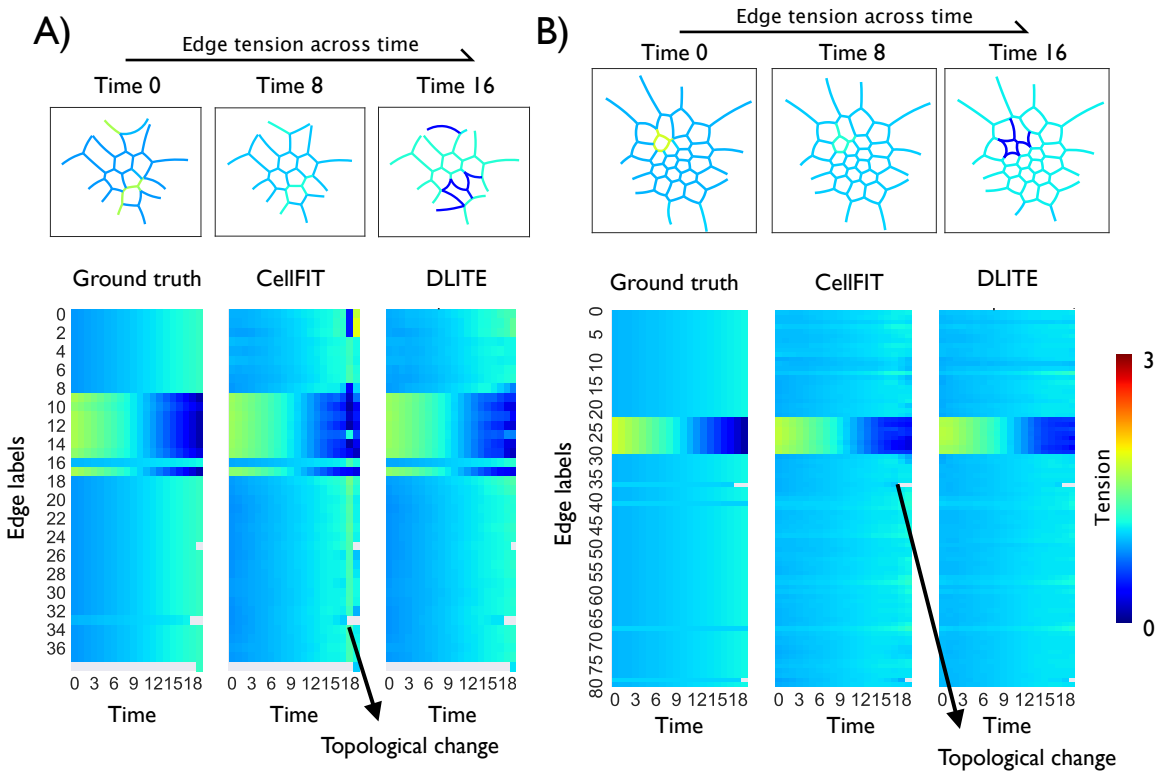

Figure S6: Two example time-series (A, B) of colony rearrangements with single topological changes (shrinkage of cell-cell junctions) at a node. Average edge tension is normalized to 1 at every time point. Shown - 3 example time points (Time 0, 8 and 16) and heatmaps of dynamic edge tensions for ground truth, CellFIT and DLITE. (A) DLITE - r = 0.97, CellFIT - r = 0.91, (B) DLITE - r = 0.975, CellFIT - r = 0.974.

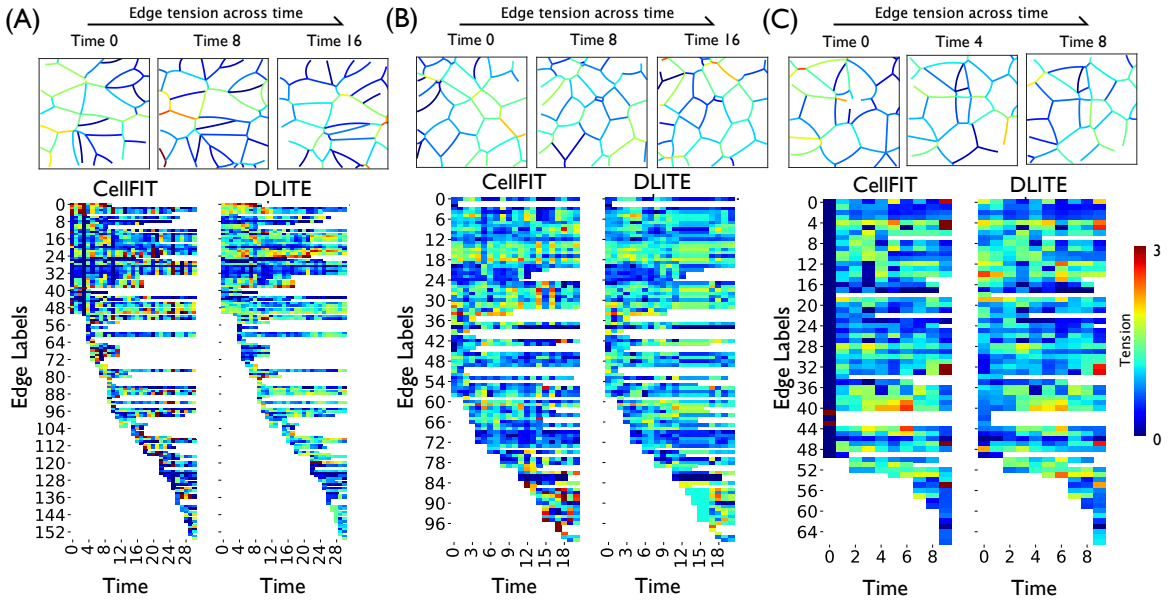

Figure S7: Predicted cell-cell forces for three scenes of ZO-1 tight junction in hIPS cells. Average edge tension is normalized to 1 at every time point. Shown - 3 example time points (Time 0, 8 and 16 or Time 0, 4 and 8) and heatmaps of dynamic edge tensions for CellFIT and DLITE.

References

1. Brugués, A. *et al.* Forces driving epithelial wound healing. *Nature physics* **10,** 683 (2014).
2. Sunyer, R. *et al.* Collective cell durotaxis emerges from long-range intercellular force transmission. *Science* **353,** 1157–1161 (2016).
3. Serra-Picamal, X. *et al.* Mechanical waves during tissue expansion. *Nature Physics* **8,** 628 (2012).
4. Du Roure, O. *et al.* Force mapping in epithelial cell migration. *Proceedings of the National Academy of Sciences* **102,** 2390–2395 (2005).
5. Ray, A. *et al.* Anisotropic forces from spatially constrained focal adhesions mediate contact guidance directed cell migration. *Nature Communications* **8,** 14923 (2017).
6. Labernadie, A. *et al.* A mechanically active heterotypic E-cadherin/N-cadherin adhesion enables fibroblasts to drive cancer cell invasion. *Nature cell biology* **19,** 224 (2017).
7. Malinova, T. S. & Huveneers, S. Sensing of cytoskeletal forces by asymmetric adherens junctions. *Trends in cell biology* **28,** 328–341 (2018).
8. Tornavaca, O. *et al.* ZO-1 controls endothelial adherens junctions, cell–cell tension, angiogenesis, and barrier formation. *J Cell Biol,* jcb–201404140 (2015).
9. Yano, T., Kanoh, H., Tamura, A. & Tsukita, S. Apical cytoskeletons and junctional complexes as a combined system in epithelial cell sheets. *Annals of the New York Academy of Sciences* **1405,** 32–43 (2017).
10. Borghi, N. & Nelson, W. J. Intercellular adhesion in morphogenesis: molecular and biophysical considerations. *Current topics in developmental biology* **89,** 1–32 (2009).
11. Chu, Y.-S. *et al.* Force measurements in E-cadherin–mediated cell doublets reveal rapid adhesion strengthened by actin cytoskeleton remodeling through Rac and Cdc42. *J Cell Biol* **167,** 1183–1194 (2004).
12. Trepat, X. & Fredberg, J. J. Plithotaxis and emergent dynamics in collective cellular migration. *Trends in cell biology* **21,** 638–646 (2011).
13. Leckband, D. E., le Duc, Q., Wang, N. & de Rooij, J. Mechanotransduction at cadherin-mediated adhesions. *Current opinion in cell biology* **23,** 523–530 (2011).

14. Rosenblatt, J., Raff, M. C. & Cramer, L. P. An epithelial cell destined for apoptosis signals its neighbors to extrude it by an actin-and myosin-dependent mechanism. *Current biology* **11,** 1847–1857 (2001).

15. Pilot, F. & Lecuit, T. Compartmentalized morphogenesis in epithelia: from cell to tissue shape. *Developmental dynamics: an official publication of the American Association of Anatomists* **232,** 685–694 (2005).

16. Rauzi, M., Verant, P., Lecuit, T. & Lenne, P.-F. Nature and anisotropy of cortical forces orienting Drosophila tissue morphogenesis. *Nature cell biology* **10,** 1401 (2008).

17. Farhadifar, R., Röper, J.-C., Aigouy, B., Eaton, S. & Jülicher, F. The influence of cell mechanics, cell-cell interactions, and proliferation on epithelial packing. *Current Biology* **17,** 2095–2104 (2007).

18. Polacheck, W. J. & Chen, C. S. Measuring cell-generated forces: a guide to the available tools. *Nature methods* **13,** 415 (2016).

19. Sugimura, K., Lenne, P.-F. & Graner, F. Measuring forces and stresses in situ in living tissues. *Development* **143,** 186–196 (2016).

20. Colom, A. *et al.* A fluorescent membrane tension probe. *Nature chemistry* **10,** 1118 (2018).

21. Gayrard, C. & Borghi, N. FRET-based molecular tension microscopy. *Methods* **94,** 33–42 (2016).

22. Grashoff, C. *et al.* Measuring mechanical tension across vinculin reveals regulation of focal adhesion dynamics. *Nature* **466,** 263 (2010).

23. Brodland, G. W. *et al.* CellFIT: a cellular force-inference toolkit using curvilinear cell boundaries. *PloS one* **9,** e99116 (2014).

24. Ishihara, S. & Sugimura, K. Bayesian inference of force dynamics during morphogenesis. *Journal of theoretical biology* **313,** 201–211 (2012).

25. Veldhuis, J. H. *et al.* Inferring cellular forces from image stacks. *Phil. Trans. R. Soc. B* **372,** 20160261 (2017).

26. Fruchterman, T. M. & Reingold, E. M. Graph drawing by force-directed placement. *Software: Practice and experience* **21,** 1129–1164 (1991).

27. Beck, A. & Ben-Tal, A. On the solution of the Tikhonov regularization of the total least squares problem. *SIAM Journal on Optimization* **17,** 98–118 (2006).

28. Jones, E., Oliphant, T. & Peterson, P. {SciPy}: open source scientific tools for {Python} (2014).

29. Blelly, A., Felipe-Gomes, M., Auger, A. & Brockhoff, D. *Stopping Criteria, Initialization, and Implementations of BFGS and their Effect on the BBOB Test Suite* in *GECCO'18 Companion* (2018).

30. Brakke, K. A. The surface evolver. *Experimental mathematics* **1,** 141–165 (1992).

31. Debnath, D., Gainer, J. S., Kim, D. & Matchev, K. T. Edge detecting new physics the Voronoi way. *EPL (Europhysics Letters)* **114,** 41001 (2016).

32. LeCun, Y., Bengio, Y. & Hinton, G. Deep learning. *nature* **521,** 436 (2015).

33. Ounkomol, C., Seshamani, S., Maleckar, M. M., Collman, F. & Johnson, G. Label-free prediction of three-dimensional fluorescence images from transmitted light microscopy. *bioRxiv.* doi:`10.1101/289504`. eprint: `https://www.biorxiv.org/content/early/2018/03/30/289504.full.pdf`. `https://www.biorxiv.org/content/early/2018/03/30/289504` (2018).

34. Attali, D. & Montanvert, A. Computing and simplifying 2D and 3D continuous skeletons. *Computer vision and image understanding* **67,** 261–273 (1997).

35. Kudelski, D., Mari, J.-L. & Viseur, S. *3D feature line detection based on vertex labeling and 2D skeletonization* in *Shape Modeling International Conference (SMI), 2010* (2010), 246–250.

36. Blonder, B., Wey, T. W., Dornhaus, A., James, R. & Sih, A. Temporal dynamics and network analysis. *Methods in Ecology and Evolution* **3,** 958–972 (2012).

37. Holgate, S. T. The airway epithelium is central to the pathogenesis of asthma. *Allergology International* **57,** 1–10 (2008).

38. Meng, G. *et al.* Injury of cell tight junctions and changes of actin level in acute lung injury caused by the perfluoroisobutylene exposure and the role of Myosin light chain kinase. *Journal of occupational health* **53,** 250–257 (2011).

39. Smoyer, W. E. & Mundel, P. Regulation of podocyte structure during the development of nephrotic syndrome. *Journal of molecular medicine* **76,** 172–183 (1998).

40. Rizzolo, L. J., Peng, S., Luo, Y. & Xiao, W. Integration of tight junctions and claudins with the barrier functions of the retinal pigment epithelium. *Progress in retinal and eye research* **30,** 296–323 (2011).

41. Fries, W., Mazzon, E., Souarzoni, S. & Martin, A. Permeability in the Rat. *Laboratory investigation* **79,** 49 (1999).

42. Mège, R.-M., Gavard, J. & Lambert, M. Regulation of cell–cell junctions by the cytoskeleton. *Current opinion in cell biology* **18,** 541–548 (2006).

43. Vasioukhin, V. & Fuchs, E. Actin dynamics and cell–cell adhesion in epithelia. *Current opinion in cell biology* **13,** 76–84 (2001).

44. Tsukita, S., Furuse, M. & Itoh, M. Structural and signalling molecules come together at tight junctions. *Current opinion in cell biology* **11,** 628–633 (1999).

45. Stephenson, R. Break, Flare, Repair: Rho Flares Locally Reinforce the Tight Junction Barrier (2018).

46. Heck, N. & Benavides-Piccione, R. Dendritic spines: from shape to function. *Frontiers in neuroanatomy* **9,** 101 (2015).

47. Evans, N. D. *et al.* Substrate stiffness affects early differentiation events in embryonic stem cells. *Eur cell mater* **18,** e13 (2009).

48. Paulin, J. J. *et al.* Large and small dendritic spines serve different interacting functions in hippocampal synaptic plasticity and homeostasis. *Neural plasticity* **2016** (2016).

49. Stevens, M. M. & George, J. H. Exploring and engineering the cell surface interface. *Science* **310,** 1135–1138 (2005).

50. Calizo, R. C. *et al.* Cell shape regulates subcellular organelle location to control short-term Ca2+ signal dynamics in VSMC. *bioRxiv,* 161950 (2018).

51. Ron, A. *et al.* Cell shape information is transduced through tension-independent mechanisms. *Nature communications* **8,** 2145 (2017).

52. Hu, M. *et al.* A biomimetic gelatin-based platform elicits a pro-differentiation effect on podocytes through mechanotransduction. *Scientific Reports* **7,** 43934 (2017).

53. Hassinger, J. E., Oster, G., Drubin, D. G. & Rangamani, P. Design principles for robust vesiculation in clathrin-mediated endocytosis. *Proceedings of the National Academy of Sciences* **114,** E1118–E1127 (2017).

54. Vasan, R., Akamatsu, M., Schöneberg, J. & Rangamani, P. in *Cell Movement* 259–301 (Springer, 2018).

55. Revell, C., Blumenfeld, R. & Chalut, K. J. Force-based three-dimensional model predicts mechanical drivers of cell sorting. *Proceedings of the Royal Society B* **286,** 20182495 (2019).

56. Herrera-Perez, R. M. & Kasza, K. E. Biophysical control of the cell rearrangements and cell shape changes that build epithelial tissues. *Current opinion in genetics & development* **51,** 88–95 (2018).

57. Spencer, A. K., Schaumberg, A. J. & Zallen, J. A. Scaling of cytoskeletal organization with cell size in Drosophila. *Molecular biology of the cell* **28,** 1519–1529 (2017).

58. Morishita, Y., Hironaka, K.-i., Lee, S.-W., Jin, T. & Ohtsuka, D. Reconstructing 3D deformation dynamics for curved epithelial sheet morphogenesis from positional data of sparsely-labeled cells. *Nature Communications* **8,** 15 (2017).

59. Diz-Muñoz, A., Fletcher, D. A. & Weiner, O. D. Use the force: membrane tension as an organizer of cell shape and motility. *Trends in cell biology* **23,** 47–53 (2013).

60. Hagberg, A., Swart, P. & S Chult, D. *Exploring network structure, dynamics, and function using NetworkX* tech. rep. (Los Alamos National Lab.(LANL), Los Alamos, NM (United States), 2008).